



Cite this: *Lab Chip*, 2023, 23, 3405

A microphysiological system for studying human bone biology under simultaneous control of oxygen tension and mechanical loading†

Julia Scheinpflug, *^{ab} Chris Tina Höfer, ^a Sarah S. Schmerbeck, ‡^a Matthias Steinfath,^a Jennifer Doka, §^a Yonatan Afework Tesfahunegn, ^e Norman Violet,^a Kostja Renko, ^a Konrad Gulich, ^a Thilo John,^c Marlon R. Schneider, ¶^a Elisa Wistorf, ^a Gilbert Schönfelder^{ad} and Frank Schulze||^{†a}

Throughout life, continuous remodelling is part of human bone biology and depends on the simultaneous action of physicochemical parameters such as oxygen tension and varying mechanical load. Thus, suitable model systems are needed, which allow concomitant modulation of these factors to recapitulate *in vivo* bone formation. Here, we report on the development of a first microphysiological system (MPS) that enables perfusion, environment-independent regulation of the oxygen tension as well as precise quantification and control of mechanical load. To demonstrate the use of the MPS for future studies on the (patho-)biology of bone, we built a simplified 3D model for early *de novo* bone formation. Primary human osteoblasts (OBs), which are the key players during this process, were seeded onto type I collagen scaffolds and cultured in the MPS. We could not only monitor cell viability and metabolism of OBs under varied physicochemical conditions, but also visualise the mineralisation of the extracellular matrix. In summary, we present a MPS that uniquely combines the independent control of physicochemical parameters and allows investigation of their influence on bone biology. We consider our MPS highly valuable to gain deeper insights into (patho-)physiological processes of bone formation in the future.

Received 23rd February 2023,
Accepted 6th June 2023

DOI: 10.1039/d3lc00154g

rsc.li/loc

Introduction

The skeleton is a highly dynamic organ, subjected to a number of internal and external stimuli that govern the

process of bone remodelling necessary for tissue growth and homeostasis.¹ Understanding the underlying mechanisms and the pathogenesis of bone remodelling defects² on a molecular and cellular level is critical for the improvement of medical treatments. Common *in vitro* cell culture approaches often neglect physicochemical properties of the tissue of interest, and may thereby miss critical aspects for cellular function,³ such as the adequate oxygen environment.⁴ As an alternative to 2D cell culture, appropriate *in vitro* models that allow the investigation of these processes under physiological conditions are being developed. Within recent years, microphysiological systems (MPS) were established to meet these requirements and to improve *in vitro* protocols.^{5–7} Until now, a variety of elaborated MPS has been published for lung, liver or kidney models, while MPS that model bone are rather underrepresented.^{5,8,9} This might reflect the fact that bone is a highly intricate tissue participating in a broad range of functions such as locomotion, protection of the inner organs, mineral homeostasis and haematopoiesis, and has been considered difficult to be recreated in its entire complexity as an *in vitro* model.⁸ However, similar to any other tissue or organ, bone physiology can be reduced to key aspects which

^a German Federal Institute for Risk Assessment, German Centre for the Protection of Laboratory Animals (Bf3R), 10589 Berlin, Germany.

E-mail: julia.scheinpflug@bfr.bund.de, Frank.Schulze2@med.uni-greifswald.de

^b Technische Universität Berlin, 13355 Berlin, Germany

^c DRK Kliniken Westend, 14050 Berlin, Germany

^d Institute of Clinical Pharmacology and Toxicology, Charité – Universitätsmedizin Berlin, Corporate member of Freie Universität Berlin, Humboldt-Universität zu Berlin, and Berlin Institute of Health, 10117 Berlin, Germany

^e Reykjavik University, 101 Reykjavik, Iceland

† Electronic supplementary information (ESI) available. See DOI: <https://doi.org/10.1039/d3lc00154g>

‡ Current address: Charité – Universitätsmedizin Berlin, Department of Neurology with Experimental Neurology, Centre for Stroke Research Berlin, 10117, Berlin, Germany.

§ Current address: Formlabs GmbH, 12459 Berlin, Germany.

¶ Current address: Institute of Veterinary Physiology, Faculty of Veterinary Medicine, University of Leipzig, Leipzig, Germany.

|| Current address: Center for Orthopaedics, Trauma Surgery and Rehabilitation Medicine, University Medicine Greifswald, 17475 Greifswald, Germany.



are vital to its functions and which might be selectively included in the model of choice to address specific research questions.

Bone consists of a multitude of cells from different lineages such as hematopoietic stem cells, endothelial cells, mesenchymal stromal cells and their respective progeny.¹⁰ In particular, osteoblasts (OBs) are key players in bone formation and bone homeostasis, while osteocytes modulate these processes in response to external stimuli such as mechanical load.^{11,12} It is well established that OBs themselves are also able to sense mechanical forces and respond by a well-orchestrated sequence of cellular activities towards full maturation and subsequent formation of bone mass.¹³ External stimuli such as low oxygen concentrations initially lead to elevated cell proliferation in bone tissue. With increasing oxygen levels and additional mechanical stimuli, OBs secrete organic and inorganic compounds, forming the extracellular matrix (ECM).^{14–17} The absence of mechanical forces leads to an arrest in bone forming activity by OBs and induces degradation of bone ECM by multinucleated osteoclasts.¹⁸ Eventually, OBs facilitate bone mineralisation, thereby transforming the tissue matrix into a structure of high mass density, rigidity and stiffness. The ECM in bone is a composite material consisting of 70% organic material, mainly type I collagen, while the inorganic phase comprises calcium and phosphate as hydroxyapatite crystals.^{19–21} This combination grants high material flexibility while providing strong resistance to plastic deformation or fracture.^{14,16}

To generate the required energy and molecular precursors for bone formation, OBs are able to perform aerobic glycolysis in addition to oxidative phosphorylation,²² *i.e.* they convert glucose into lactate independently of the presence of oxygen. This process provides energy and large numbers of metabolic intermediates that are incorporated into the ECM of bone, *e.g.* by glycosylation of type I collagen.^{23,24} This ability appears even more important when considering their native environment. Oxygen tension in bone marrow was reported to be within 6.6–8.8% (physoxia) but can go down to 1% (hypoxia) and lower, *e.g.* in the hematopoietic stem cell niche, thereby limiting oxygen-dependent processes such as mitochondrial respiration.^{25,26}

Till date, it is widely accepted that the tissue specific low oxygen tension in bone impacts the biology of resident cells.²⁷ The fundamental role of (patho-)physiological oxygen levels in human bone formation, maintenance and regeneration, albeit being recognised as vital for these processes, remains poorly understood. While the effects of mechanical loading on bone formation alone were studied in more detail both *in vivo* and *in vitro*, the interplay of oxygen tension and mechanical stimulation has not been investigated yet.^{14,28–30}

Current scientific literature indicates that, in humans, the simultaneous presence of biochemical factors such as nutrient and oxygen gradients in addition to variable mechanical loads is continuously fine-tuned to ensure bone

homeostasis.³¹ For this reason, it is necessary to develop an appropriate *in vitro* model covering both aspects, modulation of oxygen tension and mechanical loading as driving factors of bone formation. Up to now, only a few published MPS enable studies on bone biology, especially mechanobiology,³¹ while none of them provide control over perfusion, oxygen tension and mechanical loading simultaneously.⁸

In this work, we present an MPS that allows studying the influence of perfusion, oxygen environment and defined longitudinal mechanical load on three-dimensional (3D) bone tissue constructs. We used primary human OBs since these cells are vital for the formation of new bone. The OBs were seeded on a type I collagen scaffold to mimic the environment found in the early phases of *de novo* bone formation in terms of substrate stiffness. By establishing this newly engineered MPS, we were able to demonstrate that primary human OBs exhibit distinct metabolic and osteogenic responses dependent on the respective conditions, *i.e.* oxygen environment and mechanical load.

Summarising, we successfully report the use of a MPS with the unique capability to combine perfusion, regulation of oxygen tension and mechanical load for the culture of bone tissue constructs under physiologic conditions. We believe that the presented MPS will provide a deeper understanding of how these parameters interact and may influence bone regeneration and development.

Results and discussion

Design and functional characteristics of the MPS

Our MPS is based on a main unit that is connected to tubing, reservoirs and pumps for perfusion and several peripheral devices that facilitate the necessary control loops. Although this set-up is inherently complex, two trained scientists can assemble all parts. Once the system is running, it only takes one person to monitor all parameters, take daily samples and occasionally remove waste. The main unit was manufactured by injection moulding using cyclic olefin copolymer (COC), a biocompatible material.^{32,33} The optical properties of COC allowed excitation and detection of fluorescence by optical sensors like the oxygen sensor that we integrated into the system. COC further facilitated the precise control of oxygen tension within the system since the passive exchange of most gases through this material is very low.³⁴ The surface of the MPS main unit was made hydrophobic to prevent unwanted attachment and growth of cells outside the tissue construct. One main unit has the size of a microscopic slide (75.5 × 25.5 mm) and a maximum height of 20 mm. Our set-up enables the parallel operation of four MPS main units with independent control of oxygen levels and mechanical loading for each unit. Each main unit was divided into functional compartments: a gas exchange unit consisting of a fluidics chamber (in which the MPS culture medium circulates), a chamber containing the exchange gas (95% N₂, 5% CO₂) to regulate the oxygen



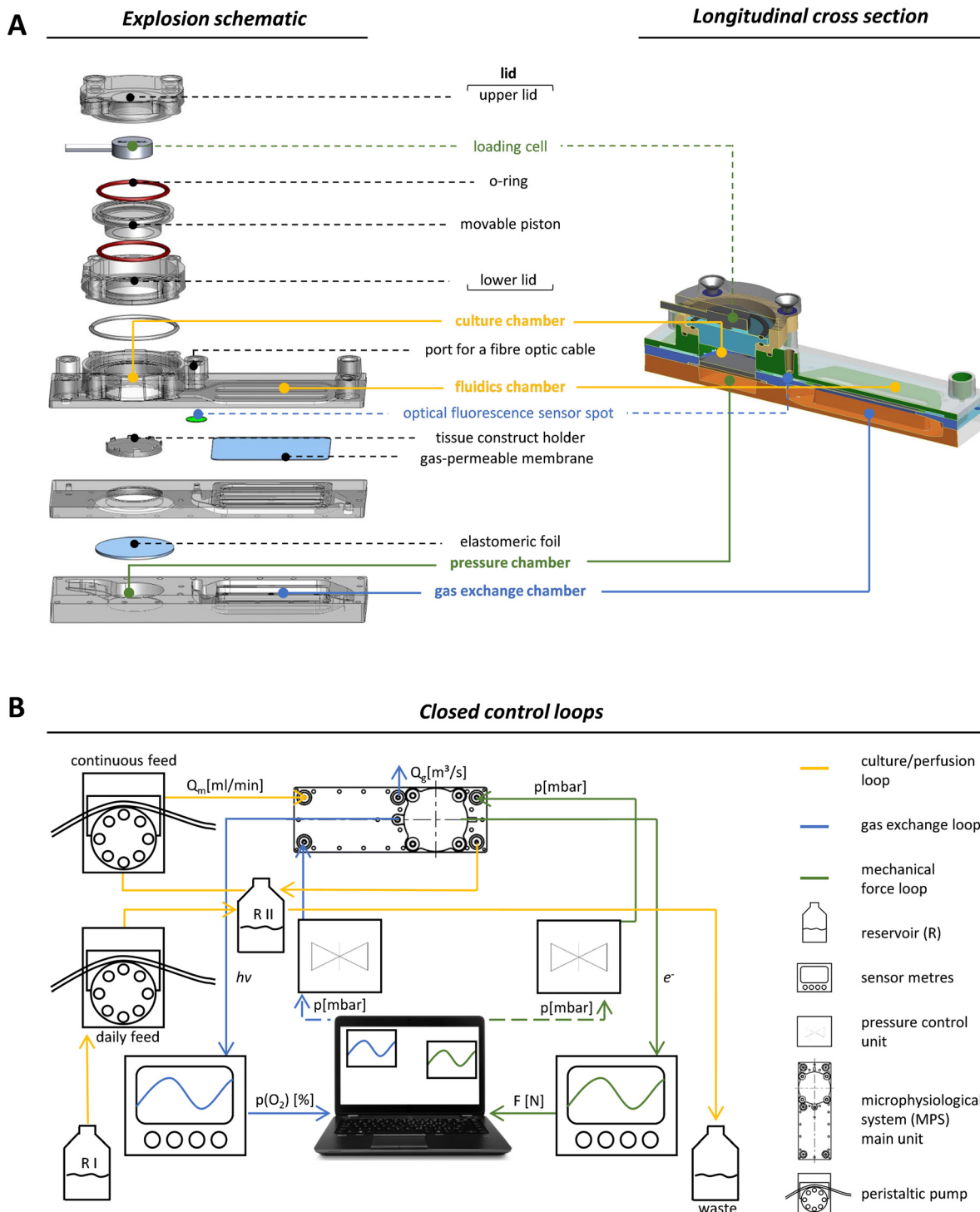


Fig. 1 Design and control of the microphysiological system (MPS). (A) Shown is an explosion schematic (left side) and a longitudinal section (right side) of the MPS main unit. All components coloured in green are involved in the application (pressure chamber) and quantification (loading cell) of the mechanical load. The yellow colour indicates all parts of the culture unit. This includes the culture chamber, where a cylindrical tissue construct can be placed, and the fluidic chamber, where the deoxygenation of the culture medium occurs. The blue colour highlights the gas exchange unit, which includes the oxygen exchange compartment and the fluorescence optical sensor that measures the oxygen tension in the MPS medium (adapted design graphic of microfluidic ChipShop GmbH). (B) Schematic representation of the mechanical loading (green) and oxygen control (blue) circuits. The culture/perfusion loop, shown in yellow, includes a closed circuit for continuous perfusion of the MPS, which is connected to an open circuit for daily medium exchange.



(Fig. 1B, green circuit). In our system, frequency and amplitude of the mechanical load can be modulated dynamically throughout (and among) experiments, to study the effects of different loading scenarios on bone formation.

Volumes of the fluidic circuit were modelled according to physiologic parameters to achieve a volume ratio between RII and the culture chamber, which corresponds to the ratio of blood to bone volume in the human body. This allows for better approximation of *in vivo* dosages when *e.g.* a drug or chemical is applied in the MPS.³⁶ The flow rate of medium was set to 0.5 mL min⁻¹, which was balanced for efficient nutrient supply and oxygen exchange.

For monitoring oxygen tension, sensor patches were integrated into the fluidic channels of the MPS main units in between the gas exchange unit and the culture chamber (Fig. 1A, blue label). Influx of oxygen into the system occurred passively by diffusion from surrounding air into the 3D printed polypropylene container RII or across the silicone tubing. In the presented system, oxygen depletion was realised as a function of the oxygen gradient between the cell culture medium compartment and the adjacent chamber for gas exchange. Once the exchange gas is pumped into the lower compartment, the diffusion of oxygen starts from the liquid phase (MPS medium) into the gas phase (exchange gas) until an equilibrium between the two phases is reached. Use of an oxygen depletion gas instead of a gas mixture with a mixing unit offered the advantage to set and adjust oxygen tension independently for each MPS main unit. While the flow rate of oxygen-free exchange gas was kept constant, the time of the gas pulses applied was varied to control the oxygen gradient and, thus, the depletion rate in the MPS medium. To find a suitable approach for the regulation of oxygen levels, we characterised the system kinetics of oxygen depletion and parameters such as response time and system inertia, but also analysed the proportionality between pulse length and depleted oxygen. We observed an asymptotic relationship between the length of applied gas pulses and the extent of oxygen depletion (Fig. 2A).

By interchanging the axes for these parameters, a proportionality factor K_p was determined by a simplified linear approximation (Fig. 2B). The K_p -value, a controller parameter, is the proportionality factor between error and controller output, in this case the pulse length. The minimal pulse length of 0.2 s was given by technical constraints. Pulse lengths of more than 3 s were found to be increasingly inefficient, which reflects the upper maximum of oxygen exchange determined by the area of the nanoporous membrane and the volume of the gas-exchange chamber (Fig. 2A). Therefore, we set the maximum pulse length to 3 s, allowing to modulate the oxygen depletion rate with pulses between 0.2 and 3 s. In between single pulses, a waiting time of 60 s was inserted. These 60 s are comprised of the system's response time and its inertia. The response time of the system, defined by the decrease of oxygen tension at the sensor spot after a pulse of exchange gas, was determined to be 6.9 s (Fig. S2A†). The system inertia was found to be comparably high with 50–60 s, which is the time that it takes for the oxygen level in the medium to reach a steady state after one single pulse (after which the influx of ambient

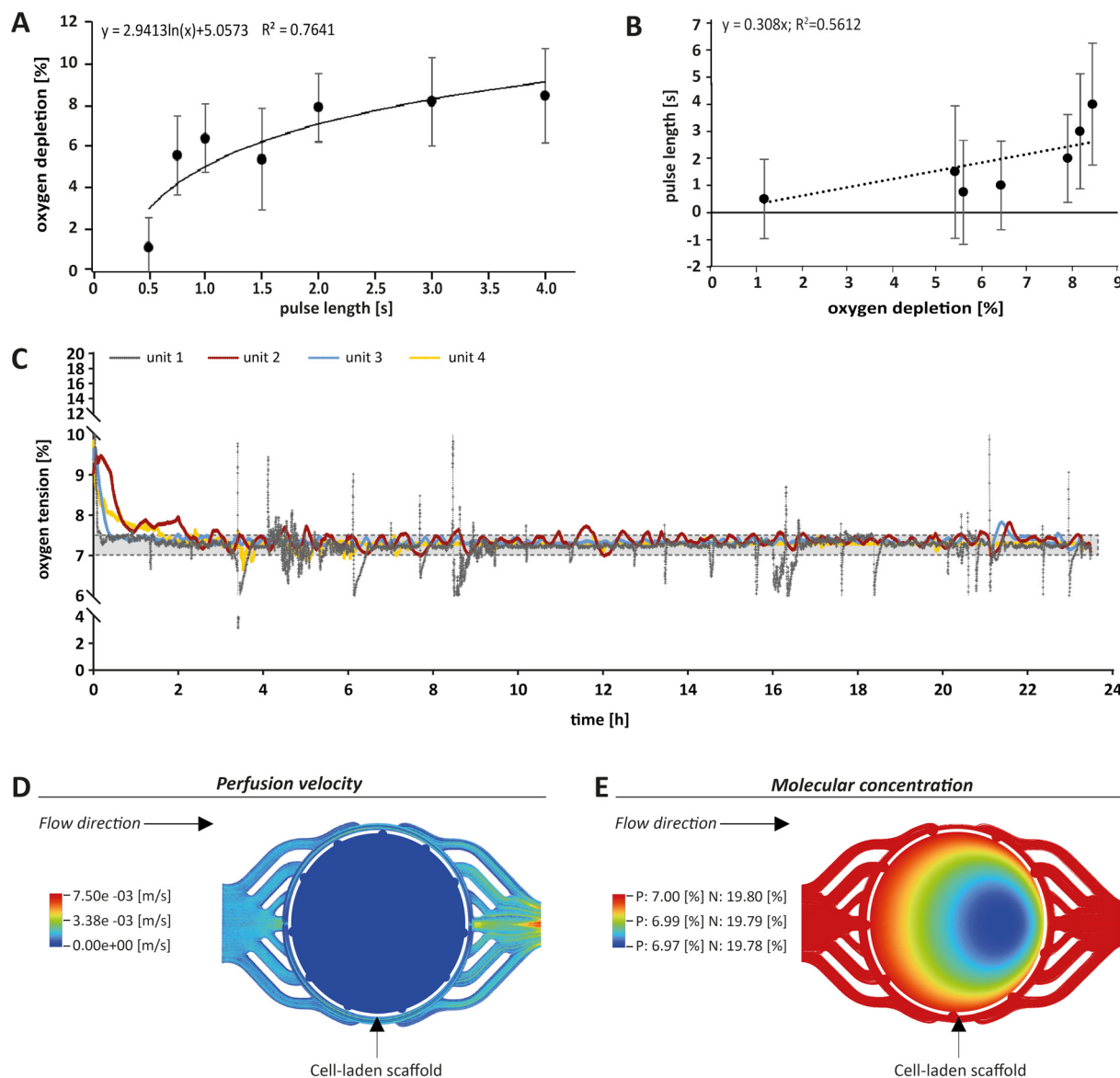


Fig. 2 Monitoring and control of oxygen tension within the MPS. (A) The pulse length of the exchange gas was plotted against oxygen depletion measured in the MPS medium. A representative graph is shown. Pulses longer than 3 s became increasingly inefficient in reducing the oxygen concentration, which is due to technical reasons. (B) Based on the control circuit shown in (A), a proportionality factor (K_p), representing the relationship between the applied pulse length of the exchange gas and the decay of oxygen tension in the MPS medium was determined. This constant corresponds to the slope of the linear approximation calculated after changing the axes for pulse length and oxygen depletion. Standard deviation was calculated from three measurements. (C) Example of an oxygen control measurement over 24 h, showing the four different MPS units in grey, red, blue and yellow. The black dashed lines indicate the range between 7% and 7.5% oxygen tension. (D) Computational fluid dynamics (CFD) modelling (Ansys Fluent 2021 R2®) of flow velocity was performed before, within and after the culture chamber containing the cell-laden scaffold (white dashed circle) and showed a drop in velocity within the culture chamber, indicating low shear stress. (E) CFD modelling of oxygen concentrations in the MPS revealed comparable oxygen gradients within the scaffold under physioxia (P) or normoxic conditions (N). With a total drop of less than 0.03% within the scaffold, this gradient is considered negligible.

oxygen from outside the MPS would slowly increase oxygen tension over time). Since the oxygen exchange dynamics of the system do not allow description by a simple mathematical model, a proportional (P)-element based control loop (Fig. S2B†) was chosen to minimise the error between target oxygen tension and measured values. The control loop ensures the delivery of exchange gas as required to achieve or maintain the set point oxygen tension over days

or weeks with a typical maximum deviation of around 0.5% from the target value (Fig. 2C) (see Experimental section “Automation of oxygen measurement by P-element based control loop” for detailed information). The chosen approach guarantees flexibility (MPS unit-independent) by free choice of the target oxygen level using a single exchange gas for depletion. Comparable systems utilised similar two-phased approaches before, yet, they relied on a pre-mixed exchange



gas with the desired oxygen concentration, aiming to establish a steady state between the liquid and the gas phase.³⁷ Supplying exchange gas for such approaches requires either a ready-to-use mixture for each use case or a gas-mixing unit and the supply of various gases in separate containers, increasing the amount of peripheral equipment needed. Therefore, our simplified and versatile approach is another step towards the implementation of oxygen control in standard experimentation. To verify the proper technical regulation of oxygen tension in our MPS, we employed a human bone osteosarcoma reporter cell line, which stably expresses a hypoxia-responsive element (HRE) fused to a luciferase reporter construct (U2OS-HRE-LUC).³⁸

This reporter cell line is therefore sensitive to low environmental oxygen tension. Consequently, we analysed U2OS-HRE-LUC under different oxygen conditions from 1% to 19.8%. As expected, we observed the highest luciferase activity following hypoxia that was adjusted within the parallelised MPS main units by the P-element-based control loop (for detailed information see Fig. S3†). Thus, our results confirmed that we are indeed able to individually adjust the oxygen level for each MPS main unit in the studied range, thereby triggering the expected cellular responses. In conclusion, our system allows analysis of cell differentiation under various conditions, including hypoxia.

To further estimate the actual oxygen exposure throughout the scaffold, we implemented a computational approach. While our MPS setup allowed for global control of oxygen tension within the MPS, we expected that oxygen levels within a tissue construct may vary due to oxygen consumption by cells and reduced passage of medium and molecules based on steric hindrance and hydrodynamic friction (viscosity) effects. Therefore, we initially used computational fluid dynamics (CFD) software to approximate fluid velocity within the culture chamber at the employed flow rate (Fig. 2D). The overall fluid velocity was found to be very low, indicating low shear stresses exerted on the cells within scaffolds cultured in the MPS. Thus, we modelled the oxygen tension inside the porous scaffold using CFD (Fig. 2E), taking into account the porosity and pore size of the scaffold and the oxygen consumption rate of OBs as reported in literature.³⁹ Our simulations indeed revealed a small gradient in oxygen levels within the scaffold when perfused with medium under normoxia (atmospheric oxygen) or physoxia. However, in these simulations the difference between the highest (19.80% or 7.00%, respectively) and the lowest oxygen level (19.78% or 6.97%, respectively) was proportionally low and within the measurement and control accuracy. Thus, according to these simulations, the oxygen gradient in the scaffold did not seem to be of relevance and can be neglected. Based on the CFD simulations, we considered the oxygenation within the perfused scaffold to be sufficient. In conclusion, the oxygen tension measured by the optical sensor spot can be used as an approximation for oxygen tension throughout the scaffold.

Design, application and control of the mechanical loading regime

In this work, we applied mechanical stimulation in form of dynamic compressive loading by pulsatile pneumatic pressure. The concept of using air pressure for mechanical stimulation was implemented in an MPS before.⁴⁰ While in the work by Park and co-workers, a two-dimensional cell layer was treated by hydrostatic pressure *via* a flexible membrane, our OBs were cultured in a dynamically compressed 3D scaffold, a situation closer to *in vivo* biomechanics. Our MPS also allowed quantification and control of the applied forces, which is a prerequisite for biomechanical investigations.⁴¹ We chose a mechanical loading pattern that has been reported to be osteoinductive. The pattern mimics physiologically relevant interfragmentary movements during fracture healing in humans due to locomotion, which typically result in 10% compression at a frequency of 1 Hz.^{28,42} We decided to apply intermittent loading alternating with periods of rest, since evidence from literature suggest that such loading intervals increase bone mass, while constant loading results in desensitisation of bone cells.^{43,44} Tissue constructs were mechanically loaded for a total of 8 h per day in 2 h loading periods, each followed by a 2 h break.

The force required to achieve a given compression of an object – such as our tissue construct – depends on the object's stiffness described by the Young's modulus.⁴⁵ In this study, commercially available type I collagen scaffolds with a known Young's modulus of 8 kPa were used that adequately model biomechanical conditions during *de novo* bone formation in processes such as regeneration.²⁷ According to this stiffness, the force needed for a 10% compressive strain was 106 mN (for detailed calculation see Fig. S4†). To ensure reproducible loading conditions in every experiment, not only the loading sensors themselves had to be calibrated, but also the relationship between applied pressure and resulting mechanical load in each newly assembled MPS main unit (Fig. 3A). Thermobonding of the MPS major components introduced micrometre-range variations affecting spatial parameters such as the culture chamber height. Therefore, each of the assembled MPS main units had to be calibrated for mechanical loading by application of small pressure bursts in the range of 0–200 mbar while recording the readout from the loading sensor. A logarithmic approximation was chosen in the relevant range to describe the effective mechanical force as a function of applied pressure (Fig. 3B). Using this function, we calculated the pressure to obtain a given mechanical load, and calibrated each MPS individually to set up the desired loading protocol.

It is noteworthy that the maximum load that can be achieved by pneumatic compression is limited and will not be suitable to study mechanical loading of adult bone with a Young's Modulus in the range of several GPa.⁴⁵ Moreover, the duration of experiments in this work was seven days, which



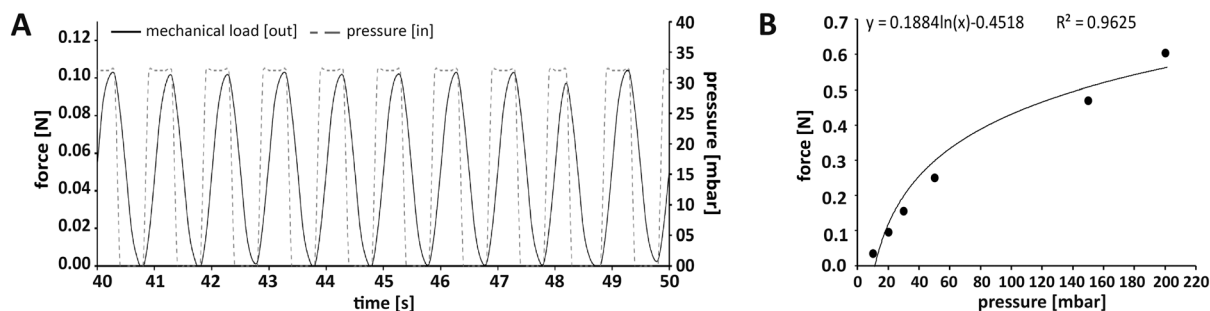


Fig. 3 Application and control of the mechanical loading regimen within the MPS. (A) Loading protocol for 10% compression at 1 Hz. In this case, the force required for 10% compression of a scaffold with a Young's modulus of 8 kPa was 106 mN (see Fig. S2† for calculation). (B) Representative plot of the relationship between the applied air pressure and the mechanical loading force that was effectively transmitted through the tissue construct and measured on its surface. A logarithmic curve was fitted to the data points to determine the pressure required for a defined loading force.

is comparably short regarding the time line of bone formation *in vivo*. Taken together, our MPS is designed for, but also limited to studies in the context of *de novo* bone formation.

Experimental setup to test the effect of mechanical loading and oxygen tension on primary bone forming cells

Depending on the model and its purpose, different cell sources can be used for bone tissue constructs. Immortal cell lines, although convenient, lack the ability to fully recapitulate the phenotype and functional spectrum of primary cells.^{46,47} Primary cells from distinct donors typically cause a considerable deviation among experiments, but, at the same time, reflect the variability found among human individuals. Therefore, primary cells are thought to be of great importance as they take genetic heterogeneity into account. Further, they have the potential to differentiate, display a tissue-specific phenotype, are non-malignant, and thus often preferred over cell lines.⁸

For initial experiments, to test the applicability of the MPS for studies on bone formation, we used a 3D model consisting of a type I collagen and 2×10^6 cells scaffold seeded with human primary OBs from four different donors (Fig. 4A, Table S1†). A representative native collagen scaffold visualised by label-free second harmonic generation (SHG) imaging prior to cell seeding is shown in Fig. 4B, and a scaffold grown with OBs in the MPS for seven days is shown in Fig. 4C. Cells, including OBs, are usually cultured and studied under normoxic conditions (standard cell culture conditions), which do not reflect the physiological oxygen tension in the body.^{4,48} Therefore, studies that aim to investigate the influence of oxygen tension on bone formation should consider physoxia. In this work, we first examined whether physoxic culture conditions in our MPS considerably alter the biology of OBs. Since mechanical loading is commonly described as the most important parameter in bone regeneration and new bone formation, we also investigated whether different effects of mechanical loading can be observed under physoxia as compared to

normoxia. Therefore, we cultured tissue constructs in the MPS under normoxia (19.8% oxygen) or physoxia (7% oxygen) in the presence and absence of mechanical loading (Fig. 4D).

Cell viability and aerobic glycolysis

To study if the applied culture conditions had an effect on the viability of OBs, we collected samples from circulating MPS medium daily. Cell death was examined for each of the four culture conditions over time (Fig. 5A and S5A†). Since the expression of lactate dehydrogenase (LDH) isoforms is sensitive to oxygen levels,^{49,50} we assessed cell viability by a protease activity assay instead. The relative protease activity in the MPS medium showed no obvious effect, indicating that culturing OBs under different test conditions did not lead to elevated cell death (Fig. 5A and S5A†). Next, we investigated cell proliferation by determining the total DNA and protein content from the cell-laden scaffolds on day seven as an approximation of cell numbers (Fig. 5B and B'). As expected, proliferation was found to vary among the donors, with donor 4 showing the overall strongest proliferation capacity. Interestingly, the application of physoxia alone did not change cell proliferation, but it tendentially increased when mechanical load was also applied (Table S2A and B†).

We also analysed the levels of mitochondrial activity, glucose and lactate to characterise cell metabolism, respectively. Mitochondrial activity was not affected by physoxia (Fig. 5C, Table S2C†). However, when mechanical load was applied additionally, we could observe a decrease in mitochondrial activity.

Furthermore, metabolism of OBs was investigated by measurements of glucose consumption and lactate production over the course of seven days. When subjected to physoxia, cells produced significantly more lactate while consuming more glucose compared to normoxia (Fig. 5D and E and S5B and D†). Mechanical load under physoxic conditions had the most pronounced effect, resulting in significantly higher levels of lactate production



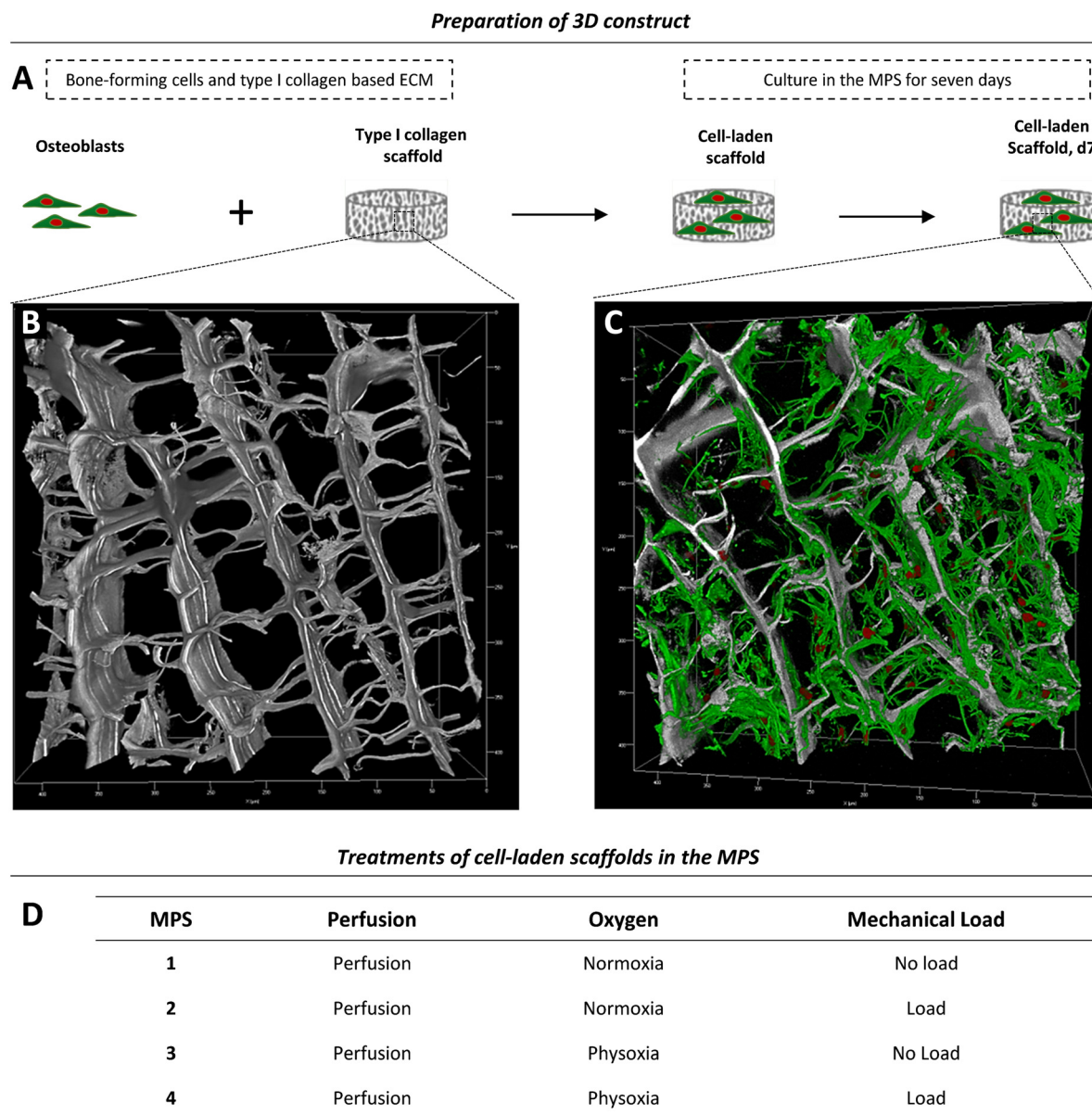


Fig. 4 Experimental setup. (A) Primary human OBs were seeded onto a type I collagen scaffold to generate a simple 3D model for osteogenesis. (B and C) Type I collagen scaffolds were imaged by second harmonic generation (SHG) and fluorescence microscopy and are shown as 3D rendering reconstructions. (B) Native collagen scaffold. The native scaffold was soaked with medium, washed and fixed prior to imaging. The collagen-specific label-free SHG signal is shown in grey. The image stack comprises a volume of $425 \times 425 \times 156 \mu\text{m}$. (C) Collagen scaffold with human OBs after seven days of incubation in the MPS under normoxia with mechanical load. Cell nuclei (red) were stained with SYTOX orange. The actin cytoskeleton (green) was stained with phalloidin-iFluor647. The image stack comprises a volume of $425 \times 425 \times 152 \mu\text{m}$. (D) Parallel experimental setup for comparison of different physiological conditions in the MPS.

(Fig. 5D and S5B; Table S2D†) and glucose consumption (Fig. 5E and S5D; Table S2E†). Lactate concentrations on day seven normalised to cell numbers revealed a slight increase under physoxic conditions in comparison to normoxia (Fig. S5C†). When normalised to total DNA on day seven, the glucose level seemed to be reduced under physoxia (Fig. S5E†), and under physoxia with mechanical load.

In summary, a reduction in glucose levels combined with an elevation of lactate concentration might indicate increased

aerobic glycolysis,²² which is an alternative pathway in OBs for the generation of energy and production of metabolites in addition to oxidative phosphorylation. In our study, only OBs that were simultaneously cultured under physoxia and mechanical loading exhibited an apparent downregulation of mitochondrial activity. This might be due to increased aerobic glycolysis and also explain the observed increase in lactate production. A study by Zeng and colleagues supports this notion, showing that lactate levels rise when glucose is consumed in MG-63 osteoblast-like cells after mechanical



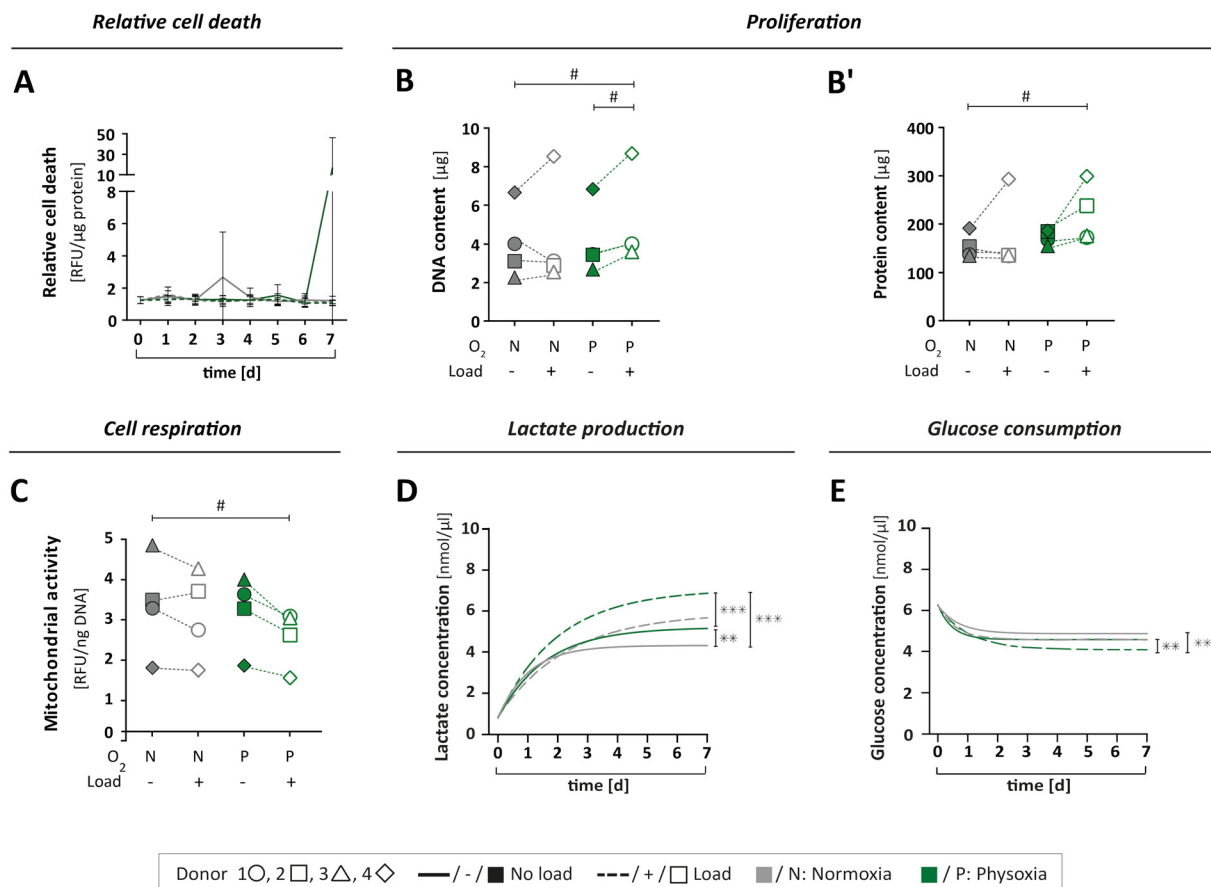


Fig. 5 Cell viability and metabolism. (A) Relative cell death was determined by measuring specific protease activity in daily samples of MPS medium over seven days, normalised to the protein content (for single value plots see Fig. S2A†). (B and B') The cell number of OBs on type I collagen scaffolds was indirectly determined by (B) DNA and (B') protein content after seven days under MPS culture conditions. (C) Cell respiration was determined by mitochondrial activity in cells after seven days in MPS culture, measured as relative fluorescence units (RFU) and normalised to the DNA content. (D) Lactate production was measured in daily medium samples over seven days for all culture conditions. (E) Glucose consumption was measured in daily medium samples for all culture conditions. (D + E) Compilation of asymptotic curves based on single values plots shown in Fig. 5B or D in one graph. All parameters were measured for the same four donors 1 ○, 2 □, 3 △, 4 ◇ ($n = 4$) either under normoxia (N) or physioxia (P), with (+/□) or without (-/■) mechanical load. Confidence intervals and p -values obtained by nonlinear mixed model analyses are given in Table S2A–E† P values < 0.005 were considered as statistically significant. Different significance levels are indicated as: # $p < 0.05$; * $p < 0.005$; ** $p < 0.0005$; *** $p < 0.0001$.

stimulation.⁵¹ The current dataset, however, is not sufficient to draw definite conclusions regarding the OB's energy metabolism. The changes observed under the different culture conditions would need further investigation such as the quantification of reactive oxygen species, amount of ATP per cell and the concentrations of metabolites other than lactate.

Taken together, neither the MPS itself nor the culture conditions applied in this work had a negative effect on cell viability, but caused distinct biological responses. The combination of physioxia and mechanical loading stimulated cell proliferation while reducing mitochondrial activity. Cell culture under physioxia led to higher glucose consumption and elevated lactate levels, which further increased significantly by application of mechanical load. Our data therefore corroborates the notion that bone cell biology strongly depends on environmental factors that are missing in standard 2D cell culture.

Extracellular matrix formation and mineralisation

To investigate the progress of functional specialisation of OBs in the tissue constructs after cultivation in the MPS for seven days, we assessed clinically relevant markers for osteogenesis. However, the obtained data varied widely between cells from different donors, which might be due to numerous differences in their medical records like age, gender, comorbidities or medications (Table S1†). The N-terminal propeptide of type I collagen (P1NP) is a clinical serum marker for bone formation, and changes in serum concentrations are highly predictive for changes in bone mass.^{52,53} We assessed P1NP in medium samples by enzyme linked immunosorbent assay (ELISA) on day seven. Measured P1NP concentrations in the culture medium were in the range of 20 to 40 ng mL⁻¹, which is the reported scale for this marker in human serum.⁵⁴ When comparing the applied culture conditions, P1NP secretion revealed donor specific



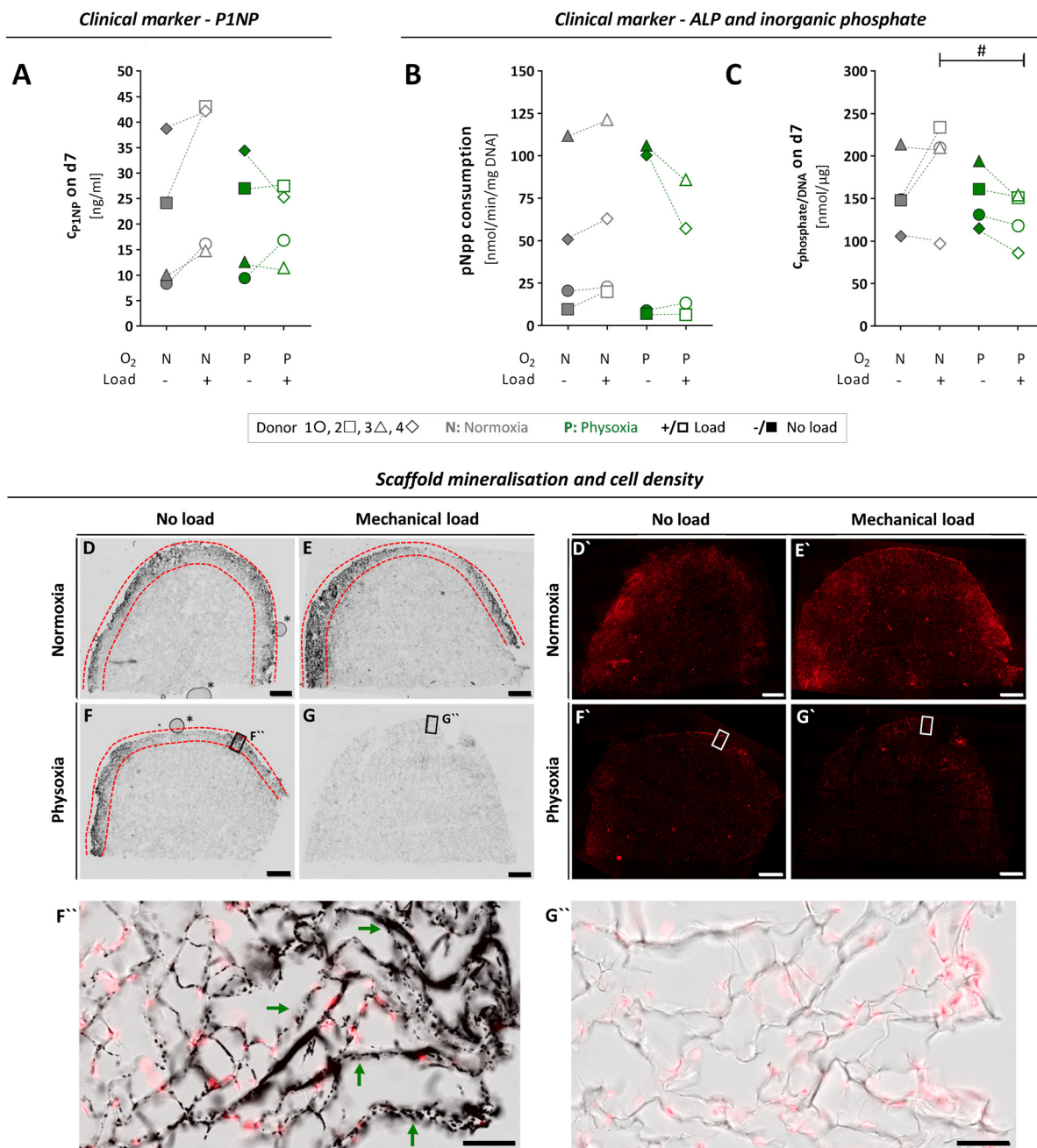


Fig. 6 Osteogenic activity of OBs, assessed by typical clinical markers and microscopic analysis of scaffold mineralisation, after seven days of culture and differential treatment in the MPS. (A) To investigate ECM formation by OBs, P1NP concentrations in the culture medium were quantified by ELISA on day seven for each culture condition. (B) ALP activity of scaffold cells was determined based on enzymatic pNpp consumption after seven days in the MPS and normalised to the DNA content. (C) Inorganic phosphate levels measured in culture medium on day seven and normalised to DNA content. (A–C) Confidence intervals and *p*-values obtained by linear mixed model analyses are given in Table S3.† *P* values < 0.005 were considered as statistically significant. Different significance levels are indicated as: # *p* < 0.05; * *p* < 0.005; ** *p* < 0.0005; *** *p* < 0.0001. All parameters were measured for the same four donors 1 ○, 2 □, 3 △, 4 ◇ (*n* = 4) either under normoxia (N) or physioxia (P), with (+/□) or without (-/■) mechanical load. (D–G) 50 μm-sections of cultivated type I collagen scaffolds were analysed comparing scaffolds grown with OBs from donor 3 under conditions of physioxia or normoxia and in the presence or absence of mechanical load. Mineralisation of type I collagen scaffolds (area between the red dashed lines) was visualised by Von Kossa staining and transmitted light microscopy, while cell nuclei (D'–G') were detected by DRAQ5 nucleic acid fluorescence staining (scale bars, 1 mm). Higher magnification images of selected regions in (F) and (G) (black frames) are shown as overlay representations of fluorescence and transmitted light images in (F'') and (G''), comparing mineralised (exemplified by green arrows) and non-mineralised regions (scale bars, 100 μm). Air bubbles (*) in (D) and (F) are inclusions of the embedding medium that had no effect on samples or staining. Additional higher magnification images from D–G can be found in Fig. S6.†



differences (Fig. 6A). It tended to increase under normoxia and mechanical load, whereby it decreased under physoxia and load, although these changes in P1NP release were not significant.

Next, we assessed mineralisation of ECM by OBs based on total alkaline phosphatase (ALP) activity of the cell-laden scaffold (Fig. 6B and C). Similar to P1NP, the enzyme ALP is a clinical serum marker that has a predictive value for bone formation in humans and can help to detect pathologies that affect this process. It is also used as a standard marker for osteogenic differentiation *in vitro*.^{55,56} First, we determined *p*-nitrophenylphosphate (*p*Npp) consumption and inorganic phosphate release as measures of ALP activity on day seven and normalised it to the total DNA content (Fig. 6B and C). We observed large variations of both parameters between individual donors and no significant changes when comparing normoxia *vs.* physoxia or mechanical load *vs.* no load (Table S3A and B†). However, application of mechanical load tend to increase ALP activity under normoxia, as shown in literature,⁵⁷ whereas it rather decreased the enzyme activity under physoxia.

To visualise mineralisation in the scaffolds after seven days of cultivation, an extra MPS run was performed with OBs from donor 3, which allowed us to preserve the intact scaffolds for histological analysis and SHG imaging. Histological staining according to von Kossa revealed mineralisation under normoxia independent of loading conditions and under physoxia if no load was applied (Fig. 6D, F and F"). In clear contrast, the application of mechanical load under physoxic conditions completely prevented mineralisation of the scaffold (Fig. 6G and G"). Nuclear staining with SYTOX orange confirmed that this was not due to a lack of cells populating the scaffold (Fig. 6D'–G'). Mineralisation on day seven was limited to the outer rim close to the scaffold surface. These observations were in line with the biochemical data on ALP activity, P1NP and inorganic phosphate concentrations of donor 3, which were highest for normoxia with mechanical load and lowest for physoxia with mechanical load (Fig. 6A–C). To date, no studies have examined mechanical loading on OBs under different oxygen tensions, making it difficult to compare our initial data. However, Matziolis and colleagues demonstrated that mechanical loading at 7 kPa at 0.05 Hz for 2 weeks stimulates osteogenic differentiation of rabbit periosteal cells under standard culture conditions (21% oxygen) with increasing type I collagen synthesis, constant ALP activity, and onset of calcification of the ECM.⁵⁸ Further, we noticed that mineralised regions frequently contained fewer cells compared to neighbouring non-mineralised regions, suggesting lower proliferation/alterd distribution or increased cell death of OBs, which is expected to occur during bone formation (Fig. 6D–F and S6A†).⁵⁹

Scaffolds cultured with OBs under the four conditions were additionally inspected by SHG and fluorescence imaging at cellular resolution. This combination of techniques allows studying both cellular organisation within scaffolds and collagen (re)organisation. Cell nuclei and the actin

cytoskeleton were fluorescently labelled, while the collagen scaffolds were detected label-free (Fig. S7, Videos S1–S4†). Major remodelling of collagen scaffolds was not observed within seven days of culture in the MPS (for none of the conditions). OBs spread within the cavities of the sponge-like scaffolds similarly under all conditions. More detailed conclusions on cell densities, cell morphologies or actin organisation are, however, not possible at this point due the small sample number.

We also examined the expression of various genes involved in osteogenesis (for detailed information see Fig. S8 and Table S4†) and mostly found an upregulation of osteogenic marker genes when cells were cultured under mechanical load as compared to the corresponding non-loaded conditions. Thus, the OB phenotype seemed to establish better under mechanical loading.

In summary, we show that primary OBs in our MPS are able to produce and mineralise ECM over seven days in culture under normoxia and physoxia. When mechanical load under physoxic conditions is applied, formation and calcification of ECM seem to be reduced in favour of proliferation, according to lower ALP activity, pro-collagen production and mineralisation. Interpretation of these results should be carried out with caution. Yet, it is known from a wealth of *in vivo* investigations that the development of the OB phenotype during bone formation involved sequential stages of cell proliferation and differentiation, leading to ECM maturation and mineralisation.⁵⁹ The initial stages of bone formation during fracture healing or development occur in an oxygen-deficient environment that gradually becomes more oxygenated as vascularisation progresses.^{60,61} Elevated proliferation of bone forming OBs at the beginning of these process is a very early osteogenic response to mechanical stimuli. It was previously shown that OB proliferation in mice induced by mechanical loading is a critical source of bone forming cells for subsequent maximal lamellar and woven bone formation.⁶² Summarising, mechanical loading seems to positively influence early osteogenesis by stimulating OB proliferation at physoxia and matrix maturation at normoxia.

We observed the expected donor-related variability of biological parameters due to the use of primary cells from donors of different age (55 to 77 years), sex, and underlying concomitant diseases (Table S1†). Albeit the apparent heterogeneity limits the scope for data interpretation, our initial experiments on early bone formation demonstrate the relevance of a MPS that independently controls physicochemical parameters. Similar to our observations regarding metabolism, we clearly demonstrated that the application of mechanical load and the control of oxygen tension had distinct effects on the bone forming ability of OBs. We therefore highlight the need to investigate cell biology under physiologic relevant conditions that are not present in standard cell culture to improve the reliability and predictive value of results. In the future, our MPS may also be suitable for a more detailed study of bone formation



SYTOX orange nucleic acid dye were purchased from Thermo Fisher Scientific (Waltham, MA, US). The CytoTox Fluor Assay Kit was received from Promega (Madison, WI, US), and the procollagen I N-terminal propeptide (P1NP) enzyme-linked immunosorbent assay (ELISA) from Elabscience (Huston, TX, US). PeqGOLD TriFAST™ for RNA purification and xylene were purchased from VWR chemicals (Radnor, PA, US). The 4% paraformaldehyde (PFA) solution (in PBS) was obtained from Alfa Aesar (part of Thermo Fisher Scientific, Lancashire, UK). Eprexia type 9 paraffin was provided by Fisher Scientific (Schwerte, Germany).

Fabrication and assembly of the MPS main unit

The MPS main unit was manufactured in collaboration with microfluidic ChipShop (Jena, Germany). The fabrication took place in a clean room. All parts of the MPS main unit (Fig. 1A) were made of cyclic olefin copolymers (COC) by injection moulding. All connections to the MPS main unit itself are compatible with LUER connectors. For oxygen measurements, an optical fluorescence sensor spot (OXSP5, Pyroscience, Aachen, Germany) was fixated with silicone glue right underneath the port for fibre optics (Fig. 1A) (see section “Oxygen measurement and control” for further details). For the oxygen exchange compartment, the nanoporous polytetrafluoroethylene (PTFE) membrane suitable for controlled gas exchange was laser cut to fit in between the lower gas exchange chamber and the upper fluidics chamber of the MPS main unit and fastened by thermo-bonding. An elastomeric COC foil was laser cut to seal the pressure chamber and was thermo-bonded in between the lower pressure chamber and upper the culture chamber. The lid of the MPS main unit was assembled manually under sterile conditions prior to the experiment as indicated in the explosion view.

The miniature load cell (ALXLC86-050G; Althen, Kellheim, Germany) was fixed in the upper part of the lid with silicone glue to monitor the mechanical load applied to the tissue construct. To ensure force transmission while sealing against the culture compartment, a movable piston is mounted in between the lid parts by two O-rings (silicone, 16 mm, 1 mm thick). Two self-tapping small screws (2.2 mm \times 5 mm) diagonally opposed to each other held the lid together. To mount the lid to the MPS main unit, another O-ring (silicone, 19 mm, 1 mm thick) was placed in a circular notch to seal the culture chamber when closed by the lid. Then, two slightly longer self-tapping screws (2.2 mm \times 9.5 mm) were used to fit into the two remaining diagonally opposite bore holes to secure the lids position. The fully assembled MPS cannot be acquired commercially. However, scientists interested in working with the MPS are welcome to contact the corresponding authors.

3D-printed peripheral components of the MPS

Some components of the MPS had to be customised and were designed using the 3D computer-aided design (CAD) software

To quantify oxygen tension, an optical fluorescence sensor spot was used. For the contactless read-out of the oxygen sensors, a fibre-optic oxygen metre was connected to the fibre optics ports on the MPS, allowing for the simultaneous readout of up to four sensors. The calibration of the oxygen measurement within the MPS units was carried out according to the manufacturers' protocol (Pyroscience, Aachen, Germany).

This journal is © The Royal Society of Chemistry 2023

was performed once a day by pumping 5.8 mL MPS medium at a flow rate of $15.7 \mu\text{L min}^{-1}$ into each of the unit reservoirs (RII) (Fig. 1B and S1A†). Excess medium was removed by outflow into 3D printed waste containers. Sampling of MPS medium was performed daily prior to exchange of medium, slowly collecting 1 mL through a silicone septum (IBIDI, Gräfelfing, Germany) integrated into the fluidic circuit using a sterile syringe and needle. Samples were stored at -80°C until further processing.

If applied, mechanical loading with 10% compression at 1 Hz was performed at regular intervals for 2 h each time alternating with a 2 h resting period during the seven days of operation (the loading script is provided as ESI†). The maximum loading time did not exceed 8 h per day. Oxygen levels in the system were constantly monitored and adjusted to either 19.8% or 7% oxygen during the entire experiment. For oxygen control, see section “Oxygen measurement and control”.

Analysis of metabolism and osteogenesis in MPS culture medium

All colorimetric and fluorimetric assays described in the following section were analysed on a Multimode microplate reader (M200 PRO; Tecan, Männedorf, Switzerland). If not stated otherwise, measurements were carried out in triplicates. To determine total protein concentration and a specific protease activity as an indicator of cell death, cryopreserved samples from the MPS culture medium were thawed on ice. Total protein concentrations were determined using the Pierce BCA Protein Assay Kit. Cell death was investigated fluorometrically using the CytoTox-Fluor Assay Kit according to the manufacturer's instructions. The fluorescence signal, as a measure for protease activity, was normalised to the total amount of protein. For analysis of metabolic and osteogenic markers, medium samples were further processed using Amicon Ultra-0.5 centrifugal filters (0.5 mL; cut-off: 10 kDa) (Merck Millipore, Burlington, MA, US). The flow-through was analysed for lactate, glucose and phosphate concentrations. The retentate was used for quantification of the amount of osteogenic marker protein P1NP. For glucose, lactate and phosphate concentrations, commercially available glucose, lactate and phosphate assay kits were employed according to the manufacturer's protocols. For the assessment of extracellular P1NP formation, human P1NP ELISA Kit was utilised according to the manufacturer's protocol.

Processing of the cell-laden scaffolds for endpoint measurements

After seven days of culture in the MPS the cell-laden scaffolds were processed for further analyses. The scaffolds were washed at least three times in 5 mL of 37°C -prewarmed DPBS, inverted several times until phenol red-free and cut into halves using a scalpel. One-half was used to determine mitochondrial activity, ALP activity, total DNA and total

protein content; the second half was used for gene expression analysis.

Quantification of mitochondrial activity, ALP activity, protein and DNA content in cell-laden scaffolds

Seven days old OB-laden scaffolds were washed as described above. Mitochondrial activity was assessed using the PrestoBlue Cell Viability Reagent according to the manufacturer's instructions with adaptations made for cell-laden scaffolds. In brief, one-half of each cell-laden scaffold was immersed in 1 mL working reagent (0.9 mL standard expansion medium supplemented with 0.1 mL PrestoBlue reagent), followed by 60 min of incubation under standard cell culture conditions. Triplicates of 200 μL of the reacted reagent were then transferred to a 48-well plate for fluorometric reading. Subsequently, cell-laden scaffolds were washed again at least three times with DPBS prewarmed to 37°C until the coloration was cleared. ALP activity was determined as described by Krause and co-authors.⁶⁵ Briefly, the scaffold halves were equilibrated in 2 mL of assay buffer (0.1 M NaCl, 0.1 M Tris, 0.001 M $\text{MgCl}_2 \times 6\text{H}_2\text{O}$ in deionised water) and then plunged into 1 mL of working solution (2.7 mM pNpp and 1 M DEA in deionised water; mixed 1:1 with assay buffer), followed by 10 min incubation under standard cell culture conditions. Scaffolds were removed from working reagent and transiently stored in 2 mL of prewarmed DPBS. To stop the enzymatic reaction, 1 mL of 1 M NaOH was added to the working solution, mixed properly, and three times 100 μL of this solution were transferred to a 96-well plate for photometric reading. Both, mitochondrial activity and ALP activity were later normalised to total DNA content. For further analysis, the cell-laden scaffolds were placed into screw-cap tubes supplemented with ceramic beads. Tubes were snap-frozen in liquid nitrogen, followed by homogenisation in a bead mill (Minilys; Bertin Instruments, Montigny-le Bretonneux, France). The whole lysate (smashed scaffold-DPBS mixture) was mixed with DPBS to a final volume of 120 μL . 3 μL of this solution were used for DNA quantification with a Cell Proliferation Assay Kit (CyQUANT) according to the manufacturer's protocol. 54 μL were mixed with 26 μL of protein extraction buffer (PEB) to prevent further degradation of proteins. PEB was prepared as described by Davis and co-authors.⁶⁶ Protein concentrations were determined in duplicates employing a Protein Assay Kit (Pierce BCA) using 25 μL of sample per measurement.

Histology

After seven days of culture in the MPS, the cell-laden scaffolds were washed as described above. Scaffolds were then cut into halves and fixed using 4% PFA solution for 10 min at RT; they were embedded in paraffin and sliced into 50 μm -sections using the manual microtome (RM 2035; Leica Microsystems, Wetzlar, Germany). Scaffold sections were transferred into 40°C -prewarmed deionised water, mounted onto HistoBond adhesive glass slides (Paul Marienfeld GmbH



detected between 638 and 735 nm. Scaffold-specific SHG signal was excited at 880 nm with a spectrally tuneable titanium-sapphire laser Chameleon Vision II (Coherent) and was detected on a forward non-descanned detector with SP485 filter (ZEISS Microscopy, Jena, Germany). Images were acquired as z-stacks at intervals of 0.87 μm in z (approx. 50% overlap of confocal planes, pinhole 40 μm) and xy -pixel size 415 nm. Maximum intensity projections and 3D surface rendering reconstructions of image stacks were generated using ZEN black software (ZEISS Microscopy, Jena, Germany) version 2.3 SP1. The imaging set-up had to be optimized to avoid considerable scaffold autofluorescence in the blue and green spectral range. Imaging depth was limited to the first 100–200 μm underneath the scaffold surface.

Statistical analysis

Both, timeline experiments (glucose, lactate, phosphate, cytotoxicity and P1NP analyses) and endpoint assays (DNA and protein determination, gene expression, ALP and mitochondrial activity analyses) were studied on four different cell donors ($n = 4$) within the MPS (1 donor = 1 MPS run). In each experiment, four different conditions were compared. For this purpose, it was investigated whether the reduction of the oxygen concentration from normoxia (19.8%) to physoxia (7%) has an influence on the cell response within the type I collagen scaffolds. Furthermore, the influence of mechanical load on the behaviour of the cells within the tissue constructs was analysed. Therefore, we assumed that the amount of glucose or lactate as a function of time ($y(t)$) can be described by an asymptotic regression model:⁶⁷

$$y(t) = \text{Asym} + (R_0 - \text{Asym})\exp(-\exp(\text{lrc})t) + \varepsilon \quad (1)$$

with

$$\text{Asym} = X\boldsymbol{\beta} + Z_1 b_{\text{don}} + Z_2 b_{\text{exp}} + Z_3 b_{\text{treat}}. \quad (2)$$

β is the vector of fixed effect coefficients, *i.e.* the vector of the treatments' impact. X describes the design matrix of the fixed effects, *i.e.*, the treatments. Z_1 and Z_2 correspond to the design matrix of the random effects due to the donors and experimental settings, respectively. Z_3 is the design matrix for the combination of donors and treatments. Here, the parameter R_0 was considered fixed for all treatments and the average of glucose or lactate on day 0 was estimated for all treatments. As described above cells from different donors were used at different experimental settings. The random coefficients are assumed to be normally distributed:

$$b_{\text{don}} \sim N(0, \sigma_b), b_{\text{exp}} \sim N(0, \sigma_{\text{exp}}), b_{\text{treat}} \sim N(0, \sigma b_{\text{treat}}), \varepsilon \sim N(0, \sigma_\varepsilon).$$

Accordingly, a nonlinear mixed model was chosen. Statistical analysis was performed using R (software) and, in particular, the R function *nlme* from the package *nlme*⁶⁷ was used to

Table 1 Overview of the parameters used for statistical analysis

Symbol	Quantity
t	Time
Asym	Asymptote
R_0	Value at time point 0
exp	Experimental setting
lrc	Slope
E	Technical variance
X	Fixed effects
β	Vector of fixed effect coefficient
Z	Random effects
1, 2, 3	Effect number
b	Random coefficient
don	Donor
treat	Treatment
N	Normal distribution
σ	Standard deviation

estimate the model parameters. The corresponding p -values were calculated from the t -value of the coefficient Asym. In this way, the asymptotic behaviour of the different treatments was compared.

No statistical model was used to evaluate cytotoxicity over culture time and PINP on day 7.

Comparison of mitochondrial activity, total DNA content, total protein amount, ALP activity, gene expression levels and day 7 normalisations was performed using a linear mixed model.

$$y = X\beta + Z_1b_{\text{don}} + Z_2b_{\text{exp}} + Z_3b_{\text{treat}} \quad (3)$$

The parameters X and Z_1 , Z_2 , Z_3 (3) were defined as already described for eqn (2). All parameters used in eqn (1)–(3) are defined in Table 1.

Author contributions

Project administration FS. Funding acquisition GS, MRS and FS. Conceptualisation FS, JS, GS and TJ. Resources GS and TJ. Methodology FS, JS and JD, YAT. Investigation JS, SSS, FS, CH, KR, KG, JD and YAT. Software FS and NV. Formal analysis MS, FS, JS. Visualisation FS, JS and CH. Writing – review & editing FS, JS, EW, CH, KR, MS, MRS, NV and GS.

Conflicts of interest

There are no conflicts to declare.

Acknowledgements

This work was supported by an internal BfR research funding program (Sonderforschungsprojekt 1322-706). In addition, this project received funding from the European Union's Horizon 2020 research and innovation programme under grant agreement No. 812954. We gratefully acknowledge our colleagues from BfR/Bf3R for scientific input and comments on the manuscript, especially Michael Oelgeschläger,

Sebastian Dunst and Aline Stolz-Ertich for constructive and scientifically valuable discussions. We thank Beate Döring, Celina Aleth, Houda Kalot and Martin Textor for excellent technical assistance. We gratefully acknowledge Prof. Margaret Ashcroft from Cambridge University, Department of Medicine, for kindly providing us the U2OS-HRE-LUC cells. We thank Jose Manuel Villarejo Ramos and Birk Urmersbach for implementing the P-element based control loop in a python-based user interface. We gratefully acknowledge microfluidic ChipShop GmbH for joint preliminary design and scientific input in the development of the MPS main unit and for providing the design drawing of the MPS main unit in Fig. 1A.

References

- 1 A. Gonciulea and S. J. de Beur, The dynamic skeleton, *Rev. Endocr. Metab. Disord.*, 2015, **16**(2), 79–91.
- 2 X. Feng and J. M. McDonald, Disorders of Bone Remodeling, *Annu. Rev. Pathol.: Mech. Dis.*, 2011, **6**(1), 121–145.
- 3 S. G. Klein, S. M. Alsolami, A. Steckbauer, S. Arossa, A. J. Parry and G. R. Mandujano, *et al.*, A prevalent neglect of environmental control in mammalian cell culture calls for best practices, *Nat. Biomed. Eng.*, 2021, **5**(8), 787–792.
- 4 V. Palacio-Castaneda, N. Velthuis, S. Le Gac and W. P. R. Verdurmen, Oxygen control: the often overlooked but essential piece to create better in vitro systems, *Lab Chip*, 2022, **22**(6), 1068–1092.
- 5 F. Zheng, F. Fu, Y. Cheng, C. Wang, Y. Zhao and Z. Gu, Organ-on-a-Chip Systems: Microengineering to Biomimic Living Systems, *Small*, 2016, **12**(17), 2253–2282.
- 6 S. N. Bhatia and D. E. Ingber, Microfluidic organs-on-chips, *Nat. Biotechnol.*, 2014, **32**(8), 760–772.
- 7 R. Kodzius, F. Schulze, X. Gao and M. R. Schneider, Organ-on-Chip Technology: Current State and Future Developments, *Genes*, 2017, **8**(10), 266.
- 8 J. Scheinpflug, M. Pfeiffenberger, A. Damerau, F. Schwarz, M. Textor and A. Lang, *et al.*, Journey into Bone Models: A Review, *Genes*, 2018, **9**(5), 247.
- 9 J. Kim, H. Lee, S. Selimovic, R. Gauvin and H. Bae, Organ-on-a-chip: development and clinical prospects toward toxicity assessment with an emphasis on bone marrow, *Drug Saf.*, 2015, **38**(5), 409–418.
- 10 B. Clarke, Normal bone anatomy and physiology, *Clin. J. Am. Soc. Nephrol.*, 2008, **3**(Suppl 3), S131–S139.
- 11 Y. Uda, E. Azab, N. Sun, C. Shi and P. D. Pajevic, Osteocyte Mechanobiology, *Curr. Osteoporos. Rep.*, 2017, **15**(4), 318–325.
- 12 A. G. Robling and L. F. Bonewald, The Osteocyte: New Insights, *Annu. Rev. Physiol.*, 2020, **82**, 485–506.
- 13 C. Ma, T. Du, X. Niu and Y. Fan, Biomechanics and mechanobiology of the bone matrix, *Bone Res.*, 2022, **10**(1), 59.
- 14 P. J. Ehrlich and L. E. Lanyon, Mechanical strain and bone cell function: a review, *Osteoporosis Int.*, 2002, **13**(9), 688–700.



- 15 N. Matsuda, N. Morita, K. Matsuda and M. Watanabe, Proliferation and differentiation of human osteoblastic cells associated with differential activation of MAP kinases in response to epidermal growth factor, hypoxia, and mechanical stress in vitro, *Biochem. Biophys. Res. Commun.*, 1998, **249**(2), 350–354.
- 16 A. Rutkovskiy, K. O. Stenslokken and I. J. Vaage, Osteoblast Differentiation at a Glance, *Med. Sci. Monit. Basic Res.*, 2016, **22**, 95–106.
- 17 O. C. Tuncay, D. Ho and M. K. Barker, Oxygen tension regulates osteoblast function, *Am. J. Orthod.*, 1994, **105**(5), 457–463.
- 18 H. K. Vaananen and T. Laitala-Leinonen, Osteoclast lineage and function, *Arch. Biochem. Biophys.*, 2008, **473**(2), 132–138.
- 19 J. A. Buckwalter, M. J. Glimcher, R. R. Cooper and R. Recker, Bone biology. I: Structure, blood supply, cells, matrix, and mineralization, *Instr. Course Lect.*, 1996, **45**, 371–386.
- 20 M. J. Glimcher, The nature of the mineral component of bone and the mechanism of calcification, *Instr. Course Lect.*, 1987, **36**, 49–69.
- 21 H. P. Wiesmann, U. Meyer, U. Plate and H. J. Hohling, Aspects of collagen mineralization in hard tissue formation, *Int. Rev. Cytol.*, 2005, **242**, 121–156.
- 22 L. Shen, G. Hu and C. M. Karner, Bioenergetic Metabolism In Osteoblast Differentiation, *Curr. Osteoporos. Rep.*, 2022, **20**(1), 53–64.
- 23 B. Flanagan and G. Nichols Jr., Metabolic Studies of Bone in Vitro. V. Glucose Metabolism and Collagen Biosynthesis, *J. Biol. Chem.*, 1964, **239**, 1261–1265.
- 24 W. C. Lee, A. R. Guntur, F. Long and C. J. Rosen, Energy Metabolism of the Osteoblast: Implications for Osteoporosis, *Endocr. Rev.*, 2017, **38**(3), 255–266.
- 25 J. S. Harrison, P. Rameshwar, V. Chang and P. Bandari, Oxygen saturation in the bone marrow of healthy volunteers, *Blood*, 2002, **99**(1), 394.
- 26 M. Jez, P. Rozman, Z. Ivanovic and T. Bas, Concise review: the role of oxygen in hematopoietic stem cell physiology, *J. Cell. Physiol.*, 2015, **230**(9), 1999–2005.
- 27 A. Petersen, A. Princ, G. Korus, A. Ellinghaus, H. Leemhuis and A. Herrera, *et al.*, A biomaterial with a channel-like pore architecture induces endochondral healing of bone defects, *Nat. Commun.*, 2018, **9**(1), 4430.
- 28 P. Klein, H. Schell, F. Streitparth, M. Heller, J. P. Kassi and F. Kandziora, *et al.*, The initial phase of fracture healing is specifically sensitive to mechanical conditions, *J. Orthop. Res.*, 2003, **21**(4), 662–669.
- 29 W. Hoffmann, S. Feliciano, I. Martin, M. de Wild and D. Wendt, Novel perfused compression bioreactor system as an in vitro model to investigate fracture healing. *Front Bioeng. BioTechniques*, 2015, **3**, 10.
- 30 M. Jagodzinski, A. Breitbart, M. Wehmeier, E. Hesse, C. Haasper and C. Krettek, *et al.*, Influence of perfusion and cyclic compression on proliferation and differentiation of bone marrow stromal cells in 3-dimensional culture, *J. Biomech.*, 2008, **41**(9), 1885–1891.
- 31 M. V. Lipreri, N. Baldini, G. Graziani and S. Avnet, Perfused Platforms to Mimic Bone Microenvironment at the Macro/Milli/Microscale: Pros and Cons, *Front. Cell Dev. Biol.*, 2022, **9**, 760667.
- 32 G. Mehta, J. Lee, W. Cha, Y. C. Tung, J. J. Linderman and S. Takayama, Hard top soft bottom microfluidic devices for cell culture and chemical analysis, *Anal. Chem.*, 2009, **81**(10), 3714–3722.
- 33 P. M. van Midwoud, A. Janse, M. T. Merema, G. M. Groothuis and E. Verpoorte, Comparison of biocompatibility and adsorption properties of different plastics for advanced microfluidic cell and tissue culture models, *Anal. Chem.*, 2012, **84**(9), 3938–3944.
- 34 E. Berthier, E. W. Young and D. Beebe, Engineers are from PDMS-land, Biologists are from Polystyrenia, *Lab Chip*, 2012, **12**(7), 1224–1237.
- 35 D. F. Gilbert, S. A. Mofrad, O. Friedrich and J. Wiest, Proliferation characteristics of cells cultured under periodic versus static conditions, *Cytotechnology*, 2019, **71**(1), 443–452.
- 36 P. G. Miller and M. L. Shuler, Design and Demonstration of a Pumpless 14 Compartment Microphysiological System, *Biotechnol. Bioeng.*, 2016, **113**(10), 2213–2227.
- 37 H. E. Abaci, R. Devendra, Q. Smith, S. Gerecht and G. Drazer, Design and development of microbioreactors for long-term cell culture in controlled oxygen microenvironments, *Biomed. Microdevices*, 2012, **14**(1), 145–152.
- 38 N. M. Chau, P. Rogers, W. Aherne, V. Carroll, I. Collins and E. McDonald, *et al.*, Identification of novel small molecule inhibitors of hypoxia-inducible factor-1 that differentially block hypoxia-inducible factor-1 activity and hypoxia-inducible factor-1 α induction in response to hypoxic stress and growth factors, *Cancer Res.*, 2005, **65**(11), 4918–4928.
- 39 H. Wang, K. D. Song, L. Wang, Y. Liu, Y. C. Liu and R. P. Li, *et al.*, Measurement of oxygen consumption rate of osteoblasts from Sprague-Dawley rat calvaria in different in vitro cultures, *Afr. J. Biotechnol.*, 2011, **10**(34), 6640–6646.
- 40 S. H. Park, W. Y. Sim, B. H. Min, S. S. Yang, A. Khademhosseini and D. L. Kaplan, Chip-based comparison of the osteogenesis of human bone marrow- and adipose tissue-derived mesenchymal stem cells under mechanical stimulation, *PLoS One*, 2012, **7**(9), e46689.
- 41 A. Petersen, P. Joly, C. Bergmann, G. Korus and G. N. Duda, The impact of substrate stiffness and mechanical loading on fibroblast-induced scaffold remodeling, *Tissue Eng., Part A*, 2012, **18**(17–18), 1804–1817.
- 42 M. Morlock, E. Schneider, A. Bluhm, M. Vollmer, G. Bergmann and V. Muller, *et al.*, Duration and frequency of every day activities in total hip patients, *J. Biomech.*, 2001, **34**(7), 873–881.
- 43 A. G. Robling, D. B. Burr and C. H. Turner, Recovery periods restore mechanosensitivity to dynamically loaded bone, *J. Exp. Biol.*, 2001, **204**(Pt 19), 3389–3399.
- 44 S. Srinivasan, S. C. Agans, K. A. King, N. Y. Moy, S. L. Poliachik and T. S. Gross, Enabling bone formation in the



- aged skeleton via rest-inserted mechanical loading, *Bone*, 2003, **33**(6), 946–955.
- 45 M. A. K. Liebschner, Biomechanical considerations of animal models used in tissue engineering of bone, *Biomaterials*, 2004, **25**(9), 1697–1714.
 - 46 G. Borciani, G. Montalbano, N. Baldini, C. Vitale-Brovarone and G. Ciapetti, Protocol of Co-Culture of Human Osteoblasts and Osteoclasts to Test Biomaterials for Bone Tissue Engineering, *Methods Protoc.*, 2022, **5**(1), 8.
 - 47 E. M. Czekanska, M. J. Stoddart, J. R. Ralphs, R. G. Richards and J. S. Hayes, A phenotypic comparison of osteoblast cell lines versus human primary osteoblasts for biomaterials testing, *J. Biomed. Mater. Res.*, 2014, **102**(8), 2636–2643.
 - 48 A. Al-Ani, D. Toms, D. Kondro, J. Thundathil, Y. Yu and M. Ungrin, Oxygenation in cell culture: Critical parameters for reproducibility are routinely not reported, *PLoS One*, 2018, **13**(10), e0204269.
 - 49 A. L. Niles, R. A. Moravec, P. Eric Hesselberth, M. A. Scurria, W. J. Daily and T. L. Riss, A homogeneous assay to measure live and dead cells in the same sample by detecting different protease markers, *Anal. Biochem.*, 2007, **366**(2), 197–206.
 - 50 J. D. Firth, B. L. Ebert and P. J. Ratcliffe, Hypoxic regulation of lactate dehydrogenase A. Interaction between hypoxia-inducible factor 1 and cAMP response elements, *J. Biol. Chem.*, 1995, **270**(36), 21021–21027.
 - 51 Z. Zeng, D. Jing, X. Zhang, Y. Duan and F. Xue, Cyclic mechanical stretch promotes energy metabolism in osteoblast-like cells through an mTOR signaling-associated mechanism, *Int. J. Mol. Med.*, 2015, **36**(4), 947–956.
 - 52 S. Vasikaran, R. Eastell, O. Bruyere, A. J. Foldes, P. Garnero and A. Griesmacher, *et al.*, Markers of bone turnover for the prediction of fracture risk and monitoring of osteoporosis treatment: a need for international reference standards, *Osteoporosis Int.*, 2011, **22**(2), 391–420.
 - 53 M. K. Koivula, L. Risteli and J. Risteli, Measurement of aminoterminal propeptide of type I procollagen (PINP) in serum, *Clin. Biochem.*, 2012, **45**(12), 920–927.
 - 54 C. Williams and A. Sapra, *Osteoporosis Markers*, StatPearls, Treasure Island (FL), 2022.
 - 55 A. Rakow, J. Schoon, A. Dienelt, T. John, M. Textor and G. Duda, *et al.*, Influence of particulate and dissociated metal-on-metal hip endoprosthesis wear on mesenchymal stromal cells in vivo and in vitro, *Biomaterials*, 2016, **98**, 31–40.
 - 56 S. Shetty, N. Kapoor, J. D. Bondu, N. Thomas and T. V. Paul, Bone turnover markers: Emerging tool in the management of osteoporosis, *Indian J. Endocrinol. Metab.*, 2016, **20**(6), 846–852.
 - 57 N. Matsuda, N. Morita, K. Matsuda and M. Watanabe, Proliferation and Differentiation of Human Osteoblastic Cells Associated with Differential Activation of MAP Kinases in Response to Epidermal Growth Factor, Hypoxia, and Mechanical Stress in Vitro, *Biochem. Biophys. Res. Commun.*, 1998, **249**(2), 350–354.
 - 58 G. Matziolis, J. Tuischer, G. Kasper, M. Thompson, B. Bartmeyer and D. Kroker, *et al.*, Simulation of cell differentiation in fracture healing: mechanically loaded composite scaffolds in a novel bioreactor system, *Tissue Eng.*, 2006, **12**(1), 201–208.
 - 59 J. B. Lian and G. S. Stein, Development of the osteoblast phenotype: molecular mechanisms mediating osteoblast growth and differentiation, *Iowa Orthop. J.*, 1995, **15**, 118–140.
 - 60 C. S. Bahney, R. L. Zondervan, P. Allison, A. Theologis, J. W. Ashley and J. Ahn, *et al.*, Cellular biology of fracture healing, *J. Orthop. Res.*, 2019, **37**(1), 35–50.
 - 61 E. Araldi and E. Schipani, Hypoxia, HIFs and bone development, *Bone*, 2010, **47**(2), 190–196.
 - 62 H. M. Zannit, M. D. Brodt and M. J. Silva, Proliferating osteoblasts are necessary for maximal bone anabolic response to loading in mice, *FASEB J.*, 2020, **34**(9), 12739–12750.
 - 63 A. Knight, Systematic reviews of animal experiments demonstrate poor human clinical and toxicological utility, *ATLA, Altern. Lab. Anim.*, 2007, **35**(6), 641–659.
 - 64 L. M. Newman, E. M. Johnson and R. E. Staples, Assessment of the effectiveness of animal developmental toxicity testing for human safety, *Reprod. Toxicol.*, 1993, **7**(4), 359–390.
 - 65 U. Krause, A. Seckinger and C. A. Gregory, Assays of osteogenic differentiation by cultured human mesenchymal stem cells, *Methods Mol. Biol.*, 2011, **698**, 215–230.
 - 66 L. A. Davis, A. Dienelt and N. I. zur Nieden, Absorption-based assays for the analysis of osteogenic and chondrogenic yield, *Methods Mol. Biol.*, 2011, **690**, 255–272.
 - 67 J. C. Pinheiro and D. M. Bates, Linear Mixed-Effects Models: Basic Concepts and Examples, in *Mixed-Effects Models in S and S-PLUS. Statistics and Computing*, ed. J. C. Pinheiro and D. M. Bates, Springer New York, New York, NY, 2000, pp. 3–56.

